Perforating artery flow velocity and pulsatility in patients with carotid occlusive disease. A 7 tesla MRI study

L.P. Onkenhout [b,1], Tine Arts [a,*,1], D. Ferro [b], E.A. Oudeman [b,d], M.J.P. van Osch [c], J.J.M. Zwanenburg [a], J. Hendrikse [a], L.J. Kappelle [b], GJ. Biessels [b], On Behalf of the Heart-Brain Connection Consortium

[a] *Department of Radiology, University Medical Center Utrecht, Heidelberglaan 100, Utrecht 3508 GA, the Netherlands*
[b] *Department of Neurology, UMCU Brain Center, University Medical Center Utrecht, Utrecht, the Netherlands*
[c] *Department of Radiology, Leiden University Medical Center, Leiden, the Netherlands*
[d] *Department of Neurology, OLVG, Amsterdam, the Netherlands*

ARTICLE INFO

ABSTRACT

Patients with carotid occlusive disease express altered hemodynamics in the post-occlusive vasculature and lesions commonly attributed to cerebral small vessel disease (SVD). We addressed the question if cerebral perforating artery flow measures, using a novel 7T MRI technique, are altered and related to SVD lesion burden in patients with carotid occlusive disease.

21 patients were included with a uni- (18) or bilateral (3) carotid occlusion (64±7 years) and 19 controls (65 ±10 years). Mean flow velocity and pulsatility in the perforating arteries in the semi-oval center (CSO) and basal ganglia (BG), measured with a 2D phase contrast 7T MRI sequence, were compared between patients and controls, and between hemispheres in patients with unilateral carotid occlusive disease. In patients, relations were assessed between perforating artery flow measures and SVD burden score and white matter hyperintensity (WMH) volume.

CSO perforating artery flow velocity was lower in patients than controls, albeit non-significant (mean difference [95% confidence interval] 0.08 cm/s [0.00–0.16]; $p = 0.053$), but pulsatility was similar (0.07 [-0.04–0.18]; $p = 0.23$). BG flow velocity and pulsatility did not differ between patients and controls (velocity = 0.28 cm/s [-0.32–0.88]; $p = 0.34$; pulsatility = 0.00 [-0.10–0.11]; $p = 0.97$). Patients with unilateral carotid occlusive disease showed no significant interhemispheric flow differences. Though non-significant, within patients lower CSO ($p = 0.06$) and BG ($p = 0.11$) flow velocity related to larger WMH volume.

Our findings suggest that carotid occlusive disease may be associated with abnormal cerebral perforating artery flow and that this relates to SVD lesion burden in these patients, although our observations need corroboration in larger study populations.

1. Introduction

Patients with uni- or bilateral carotid occlusive disease are known to express post-occlusive hemodynamic abnormalities in the cerebral vasculature. These include a lower perfusion pressure in the absence of sufficient collaterals [1,2] as well as abnormalities in cerebral blood flow (CBF) and cerebrovascular reactivity [3–7]. Furthermore, patients may develop low-flow infarcts, mainly in border zone areas of the brain, the deep white matter (WM) of the semi-oval center (CSO), and the gray matter of the basal ganglia (BG) [1,3,7–9]. Moreover, patients with carotid occlusive disease can also express lesions typically attributed to small vessel disease (SVD), such as lacunar infarcts and white matter hyperintensities (WMH) [9]. It has been suggested that the burden of these lesions is higher at the ipsilateral side of the occlusion or stenosis, although results from previous studies are conflicting [10,11]. This raises the question if hemodynamics of small vessels, in particular in perforating arteries, are also affected in patients with carotid occlusive disease.

---

* Corresponding author.
  E-mail address: t.arts-4@umcutrecht.nl (T. Arts).
[1] These authors contributed equally to this work.

With the advance of 7 tesla (T) MRI we are now able to measure blood flow velocity and pulsatility in the small perforating arteries of the brain [12]. In this study, we assessed if perforating artery flow measures are altered in patients with carotid occlusive disease. We compared flow velocity and pulsatility in the cerebral perforating arteries in the CSO and BG between patients with carotid occlusive disease and matched controls, as well as interhemispherically in patients with unilateral carotid occlusive disease. In addition, we investigated if perforating artery flow measures are related to lesions typically attributed to SVD.

2. Materials and methods

2.1. Study population

Participants of the Heart Brain Connection study were included and all participants provided written informed consent prior to enrolment in the study [13]. We included participants with asymptomatic or symptomatic > 80% stenosis of the internal carotid artery (ICA) who were not eligible for a carotid endarterectomy, as well as patients with an occlusion of the ICA. Patients with an ICA occlusion should not have had a brain infarct or transient ischemic attack in the three months prior to inclusion. Subjects in the control group had no history of carotid occlusive disease. All participants were aged > 50 years and independent in daily life and had a 7T MRI available, acquired according to protocol (for all in- and exclusion criteria we refer to Table 1). Patients and controls were matched for age and sex through frequency matching. All participants underwent clinical evaluation, a 3T brain MRI [13] and within three months a 7 tesla MRI. We obtained informed consent in 58 participants, four were excluded due to claustrophobia, seven dropped out due to errors with the scanner at the study visit and inability to reschedule the participant. In 21 patients with carotid occlusive disease and 19 controls the 7T MRI scans were successfully obtained (for more details we refer to Fig. 1).

The Heart-Brain Connection study was approved by the Medical Ethics Committee of the Leiden UMC (LUMC) and local boards of the participating UMCs (LUMC, Maastricht UMC, Utrecht UMC and VU UMV) [14]. The study was conducted in accordance with the declaration of Helsinki and the Medical Research Involving Human Subjects Act (WMO).

Table 1

Inclusion and exclusion criteria of patients with carotid occlusive disease and controls.

General selection criteria
Inclusion criteria
Age 50 years or older
Able to undergo cognitive testing
Independence in daily life
Exclusion criteria
Contraindication for MRI or unable to undergo MRI protocol due to physical condition
Life-threatening disease with life expectancy less than 3 years other than carotid occlusive disease
Participation in ongoing trials for therapeutic interventions including randomized controlled trials and clinical trials of investigational medicinal products
Additional selection criteria for patients with carotid occlusive disease
Inclusion criterion
Significant stenosis (>80%) or occlusion of the internal carotid artery as visible on MR angiography
Exclusion criteria
Plan for carotid surgery
Brain infarct or transient ischemic attack in the three months prior to inclusion
Additional selection criteria for controls
Inclusion criteria
n/a
Exclusion criterion
A diagnosis of carotid occlusive disease

Showing the selection criteria relevant to our study. For more elaborate in- and exclusion criteria on the overall Heart Brain Connection study we refer to the design article. [14].

2.2. Clinical characteristics

For the patients with carotid occlusive disease the side of the stenosis or occlusion was recorded and whether the stenosis or occlusion had been symptomatic, which was defined as a transient ischemic attack (TIA) or ischemic stroke. This was based on medical records and questionnaires. Possible stenosis or occlusions in other cervical arteries (i.e. left and right internal carotid arteries and left and right vertebral arteries) were recorded from medical records as well.

Vascular risk factors were recorded for patients and reference participants. Hypertension was determined by measurement on two study visits. Each study visit systolic and diastolic blood pressure were measured on each arm twice, at least one minute apart. Mean systolic and diastolic blood pressure were averaged out of four measurements on two study visits. The criteria for hypertension were: the use of blood pressure medication, or a mean systolic blood pressure above 140 mmHg or a mean diastolic blood pressure higher than 90 mmHg. The criteria for hyperlipidemia were: the use of cholesterol lowering medication, or a diagnosis of hyperlipidemia by a physician based on earlier blood cholesterol and LDL levels (even if a patient did not use medication, but for example would adhere to a diet) or a present LDL above 3,5 mmol/L. The present LDL cholesterol level (mmol/L) was determined from a blood sample taken from the participant the first study visit. The criteria for diabetes were: the use of antidiabetic medication, or a diagnosis of diabetes by a physician (even if a patient did not use medication, but for example would adhere to a diet) based on glucose levels or on previous or present HbA1c levels above 53 mmol/mol. The present HbA1c level (mmol/mol) was determined from a blood sample taken from the participant at the first study visit. Both current and previous smoking was noted, as well as the number of years of smoking, years stopped and amount of smoked cigarettes/cigars per day.

2.3. Image acquisition

2D phase contrast (PC) acquisitions aimed at small perforating arteries in the semioval center (CSO) and the basal ganglia (BG) were performed on 7T MRI (Philips) as previously described [12,15]. Slice planning and scanning parameters of the 2D PC scans are shown in Fig. 2 and Table 2. Of note, slice planning of the phase contrast acquisitions was individually adapted, based on a T1 image. In addition, 2D-Qflow measurements at the first branch of both left and right middle cerebral arteries (MCA, M1) were acquired. A peripheral pulse oximeter was used for retrospective gating and cushions were placed beside the subject's head to minimize head movement during scanning.

2.4. Image processing

2.4.1. First segment of the middle cerebral artery (M1)

Velocity (cm/s) and pulsatility measurements at the first segment of both left and right middle cerebral arteries were acquired on 7T MRI (0.5×0.5 mm resolution, Venc=120 cm/s) using a 2D-Qflow sequence. Contouring of the M1 was done semi-automatically using MeVisLab (v3.1.1, VS2017, MeVis Medical Solutions AG, DE) and M1 flow velocity was defined as the average over the contoured lumen. Pulsatility was derived from the velocity (V) using the following formula

$$pulsatility = (V_{max} - V_{min})/V_{mean} \tag{1}$$

where V_{max}, V_{min} and V_{mean} are the maximum, minimum and mean flow velocity, respectively. Flow velocity and pulsatility measures of left and right M1 were averaged. During data analysis we learned that the echo time of the M1 2D-Qflow was too long, resulting in flow voids. Due to this problem data of three participants with flow voids covering a large part of the contoured lumen were not used in the analyses.
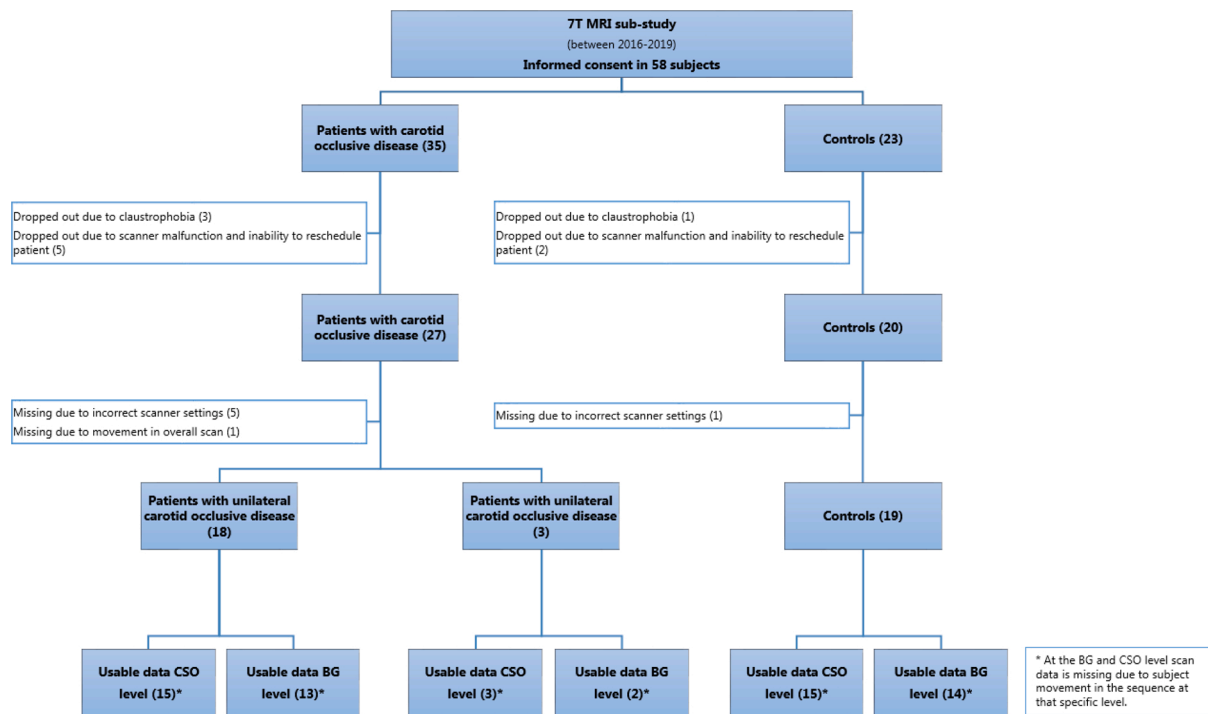
Fig. 1. Flow-chart showing the number of excluded participants and final numbers of phase contrast scans for patients and controls.
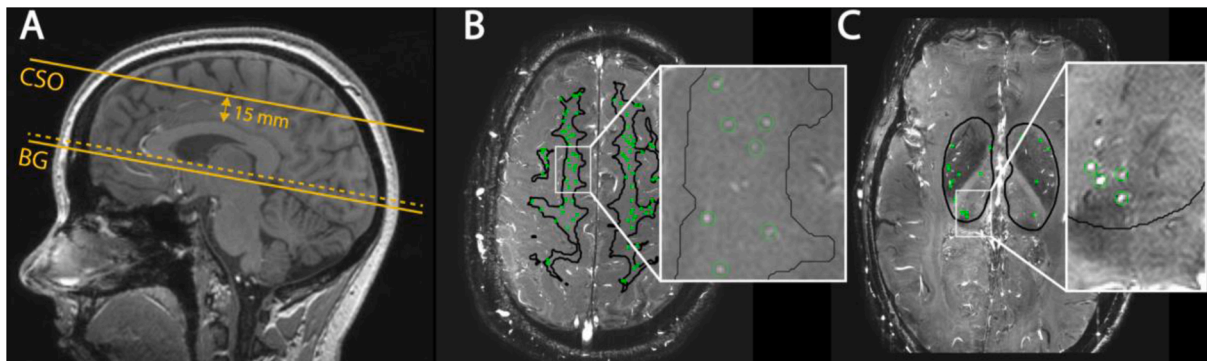

Fig. 2. Planning of the two-dimensional (2D) quantitative flow (Qflow) slices and regions of interest (ROIs). (A) Planning of the basal ganglia (BG) and semioval center (CSO) slices on a sagittal T1-weighted image. The slice planning is indicated by the yellow lines. For the BG a 2D slice is planned through the anterior commissure, parallel to the genu aligned to the splenium of the corpus callosum (dotted line) and aligned in the horizontal plane for the left/right axis; CSO planning is parallel to the BG plane located 15 mm above the corpus callosum. (B) ROI (black line; see methods for details) on the 2D Qflow image in the CSO slice, cerebral perforating arteries detected circled in green. (C) ROI in the BG slice, cerebral perforating arteries detected circled in green.

2.4.2. Cerebral perforating arteries

2D PC scans were first visually checked for sufficient quality; scans with poor image quality due to severe subject movement were excluded from analysis.

Perforating artery flow measures were assessed in the two regions of interest using a 2D WM mask at the CSO and a manual delineation of the BG, both excluding infarcts [15]. WM masks and lacunar infarcts in these regions were delineated from 3T MRI T1-weighted and FLAIR images using the Quantib Brain Segmentation Tool and the FMRIB Software Library (FSL version 6.0.1, Oxford, UK)(Sup. Table 1) [16]. The lacunar infarct masks were dilated with a 3×3 mm kernel. The dilated lacunar infarcts were removed from the WM mask, and the resulting mask was further eroded by including only the central white matter, which was defined as white matter further than 16 mm away from the outer edge of the brain. This additional erosion was performed because the poor gray/white matter contrast in these regions on the PC image makes it difficult to recognize a mismatch between the WM mask

and the underlying anatomy as described before [17]. Small perforating arteries in the CSO and BG were detected as previously published [15], also automatically excluding CSO perforating arteries located in ghosting artifact regions [17] and perforating arteries in the BG oriented non-perpendicularly to the scanning plane. In addition, apparent perforating arteries located within a 1.2 mm radius from each other were excluded, as these are mostly multiple detections located on larger and/or non-perpendicular vessels (Fig. 2). Of note, the 2D WM masks where not limited to the perfusion territory of the carotid artery. Our technique does not permit separating perforating arteries fed by the carotids from those fed by the vertebrobasilar system. Yet, based on the vascular anatomy, the majority of the included vessels should originate from the carotids, although this can vary between subjects, also due to collateral flow in the patients.

The perforating artery density, mean blood flow velocity and pulsatility were assessed separately for the BG and CSO. The cerebral perforating artery density is defined as the number of perforating

Table 2

Imaging parameters of the 2D phase contrast sequence in CSO and BG.

	2D PC CSO/BG
FOV, mm (RLxAP)	$250 \times 250/250 \times 169$
Slices	1
Acquired voxel size, mm*	$0.3 \times 0.3 \times 2.0$
Flip angle**,°	50–90/60
Venc, cm/s	4/20
TR, ms	28.5–29.6/28
TE, ms	16.1–17.3/14.7–15.0
TFE factor	2
Sense factor (AP direction)	1.5/1
Acquired time points	10–15/11–15
Scan time, min:s***	3:30/3:32
*** scantime for a heart rate of 80 bpm	

Imaging parameters of the 2D phase contrast sequence in the semi-oval center (CSO) and basal ganglia (BG). Abbreviations: PC = phase contrast; FOV = field of view; RL = right-left, AP = anterior-posterior; Venc = encoded velocity; TR = repetition time; TE = echo time; TFE = turbo field echo. *Reconstructed to 0.2×0.2 mm2 in-plane resolution. ** Ramped flip angle along the flow direction (perpendicular to the slice) to mitigate saturation effects.

arteries per cm^2 of the mask. Averaging over all perforating arteries results in the mean blood flow velocity. To calculate the pulsatility the perforating arteries' velocity curves are first normalized by division with V_{mean} and averaged before the pulsatility is calculated using formula [1] (due to the normalization procedure V_{mean} equals 1.0).

2.5. SVD manifestations

Automated delineation of WMH was based a previous method using a FLAIR scan (sup. Table 1 and sup. Fig. 1). [18] Visual assessment of lacunar infarcts, microbleeds, enlarged perivascular spaces, and WMH grade was performed by a neuroradiologist. SVD burden score ranged 0–4, and was based on i) presence of one or more lacunar infarcts (1 point), ii) microbleeds present (1 point), iii) moderately to severely enlarged perivascular spaces in basal ganglia (1 point), iv) Fazekas 3 (1 point), according to an established scale. [19,20] To limit the number of correlational analyses perforating artery flow measures were primarily related to WMH volume and the SVD burden score.

2.6. Statistical analysis

Demographics and vascular risk factors were compared between patients and controls with unadjusted independent *t*-test or Chi square test for proportions. Perforating artery flow measures were compared between the groups with ANOVA, in secondary analyses also adjusted for age, sex and hypertension. In patients with unilateral carotid occlusive disease, flow measures were compared between hemispheres with paired samples t-tests. In the patients, the relation between perforating artery flow measures and SVD manifestations was assessed with Spearman correlation. All data analyses were executed in IBM SPSS statistics (v. 22, SPSS Inc., Chicago, IL) and a *p*-value ≤0.05 was considered statistically significant. With the achieved sample size of 21 patients and 19 controls the study was powered to detect differences between the groups with an effect size ≥0.9 SD units for continuous variables (alpha 0.05, power 80%).

3. Results

Of 27 patients with carotid occlusive disease and 20 controls, 21 patients and 19 controls (mean age) had sufficient 2D PC scan quality at the CSO or BG level, and these 40 subjects constituted the study population (characteristics in Table 3). The reason for low quality scans were artifacts resulting from subject movement during scanning. Among the 40 study subjects, patients and controls were well matched for age (mean age 64±7 years, 65±10 years, respectively), but among the

Table 3

Demographics, vascular risk factors and small vessel disease manifestations in patients with carotid occlusive disease vs. controls.

	COD	controls	*p*
Demographics			
Age	64±7	65±10	0.74
Sex (male)	15 (71)	9 (47)	0.12
Unilateral ACI occlusion	18 (86)	N.a.	
Vascular risk factors			
Hypertension	16 (76)	4 (21)	<0.01
Hypercholesterolemia	19 (90)	6 (32)	<0.01
Diabetes mellitus	5 (23)	0 (0)	<0.01
Current smoking	6 (29)	2 (11)	0.08
History of reported TIA	15 (71)	0 (0)	<0.01
History of reported ischemic stroke	11 (52)	0 (0)	<0.01
Small vessel disease manifestations			
SVD burden score [0–4]	1 [0; 2]	0 [0; 1]	0.25
WMH volume (ml)	0.54 [0.28; 1.7]	0.27 [0.11; 0.73]	0.11
Lacunar infarct (number present)	1 [0; 2]	0 [0; 0]	0.00
Microbleeds (number present)	0 [0; 0]	0 [0; 0]	0.41

Demographics are listed of 21 patients with carotid occlusive disease and 19 controls, unless indicated otherwise. Data presented as group mean ± standard deviation or n (%). Age and $N_{detected}$ were compared with a Student's *t*-test, all other demographic and vascular risk factor comparisons with a Chi square test. Small vessel manifestations are compared using a Mann Whitney U analysis, and results are presented as median [quartile: 25%; 75%]. Abbreviations: COD = carotid occlusive disease; ACI = internal carotid artery; SVD = small vessel disease; WMH = white matter hyperintensity.

patients the proportion of males was higher (15 (71%) versus 9 (47%)). The carotid occlusion was unilateral in 18 patients and bilateral in three.

Sixteen patients and four controls were diagnosed with hypertension (Table 2). Four patients were diabetic. Fifteen patients were symptomatic, of which eleven with ischemic stroke, and fifteen with TIA.

M1 velocity and pulsatility measures could be obtained of 18 patients and 19 controls. Exclusion was necessary because of flow voids. M1 flow velocity was not significantly different between patients with carotid occlusive disease (34.1 ± 10.8 cm/s) and controls (34.9 ± 7.8 cm/s) (mean difference [95% CI]=0.8 cm/s [-5.5 – 7.1], $p = 0.39$). The same was found for pulsatility between patients (0.79 ± 0.25) and controls (0.65 ± 0.32)(0.14 [-0.04 – 0.31], $p = 0.12$). In patients with carotid occlusive disease no differences were found for M1 velocity between the ipsilateral (34.8 ± 10.9 cm/s) and contralateral hemisphere (36.2 ± 8.8 cm/s)(1.38 cm/s [-4.92 – 7.69], $p = 0.65$). M1 pulsatility was significantly lower in the ipsilateral hemisphere (0.74 ± 0.26) compared to the contralateral hemisphere (0.82 ± 0.27)(0.08 [-0.00 – 0.16], $p = 0.049$).

3.1. Perforating artery flow measures of patients with carotid occlusive disease vs. controls

In the CSO, $N_{density}$ and pulsatility of the perforating arteries were similar in patients with carotid occlusive disease as compared to controls, but flow velocity tended to be lower in patients (mean difference [95%CI]: 0.08 cm/s [0.00 – 0.16], $p = 0.053$). In the BG, $N_{density}$, flow velocity and pulsatility were similar between patients and controls (Table 4). Adjustment for age, sex, smoking status and hypertension did not influence these results.

3.2. Perforating artery flow measures between hemispheres of patients with carotid occlusive disease

In the 18 patients with unilateral carotid occlusive disease there were no differences in Ndensity or the perforating artery flow measures between hemispheres in the CSO (Table 5). In the BG, perforating artery flow velocity and Ndensity also did not differ between hemispheres. However, BG perforating artery pulsatility tended to be lower in the ipsilateral than the contralateral hemisphere (0.11 [-0.00 – 0.22], $p = 0.08$).

Table 4
Cerebral perforating artery flow in carotid occlusive disease patients and controls.

	COD	controls	mean difference [95% CI]	p#	p*
$N_{detected}$ CSO	40 ± 22 (n = 18)	33 ± 24 (n = 15)	−7.5 [−23.6 – 8.7]	0.35	0.12
$N_{detected}$ BG	16 ± 3 (n = 15)	17 ± 6 (n = 14)	0.6 [−2.9 – 4.1]	0.74	0.40
Ndensity CSO (#/cm2)	2.3 ± 0.91 (n = 18)	2.6 ± 1.0 (n = 15)	0.32 [−0.22 – 0.85]	0.61	0.94
Ndensity BG (#/cm2)	0.69 ± 0.18 (n = 15)	0.69 ± 0.26 (n = 14)	0.00 [−0.14 – 0.14]	0.93	0.13
Flow velocity CSO (cm/s)	0.66 ± 0.12 (n = 18)	0.74 ± 0.11 (n = 15)	0.08 [0.00 – 0.16]	0.053	0.29
Flow velocity BG (cm/s)	3.45 ± 0.66 (n = 15)	3.73 ± 0.90 (n = 14)	0.28 [−0.32 – 0.88]	0.34	0.38
Pulsatility CSO	0.40 ± 0.16 (n = 18)	0.47 ± 0.15 (n = 15)	0.07 [−0.04 – 0.18]	0.23	0.21
Pulsatility BG	0.41 ± 0.13 (n = 15)	0.41 ± 0.14 (n = 14)	0.00 [−0.10 – 0.11]	0.97	0.50

Data are presented as group mean ± standard deviation. # ANOVA test, unadjusted. * ANCOVA test, adjusted for age, sex, smoking and hypertension. Abbreviations: COD = carotid occlusive disease; $N_{detected}$ = the number of detected perforating arteries; Ndensity = number of detected cerebral perforating arteries/cm2; CSO = semioval center; BG = basal ganglia; CI = confidence interval.

Table 5
Cerebral perforating artery flow in the hemisphere ipsilateral and contralateral to the carotid occlusion.

	hemisphere ipsilateral to the occlusion	hemisphere contralateral to the occlusion	mean difference [95% CI]	p#
$N_{density}$ CSO (#/cm^2)	2.09 ± 1.01 (n = 15)	2.57 ± 1.15 (n = 15)	0.48 [−0.06 – 1.02]	0.08
$N_{density}$ BG (#/cm^2)	0.79 ± 0.35 (n = 13)	0.60 ± 0.19 (n = 13)	−0.19 [−0.44 – 0.06]	0.20
Flow velocity CSO (cm/s)	0.63 ± 0.18 (n = 15)	0.66 ± 0.12 (n = 15)	0.03 [−0.04 – 0.11]	0.41
Flow velocity BG (cm/s)	3.49 ± 0.82 (n = 13)	3.47 ± 0.73 (n = 13)	−0.02 [−0.46 – 0.42]	0.92
Pulsatility CSO	0.50 ± 0.23 (n = 15)	0.46 ± 0.19 (n = 15)	- 0.04 [−0.19 – 0.11]	0.57
Pulsatility BG	0.44 ± 0.12 (n = 13)	0.56 ± 0.17 (n = 13)	0.11 [−0.00 – 0.22]	0.08

Results are shown for 18 patients with unilateral carotid occlusive disease. Data are presented as group mean ± standard deviation. # paired samples *t*-test. Abbreviations: $N_{density}$ = number of detected cerebral perforating arteries/cm^2; CSO = semioval center; BG = basal ganglia; CI = confidence interval.

3.3. SVD manifestations and relations with perforating artery flow measures

Compared to controls, patients with carotid occlusive disease showed significantly more lacunar infarcts (patients=1 [0;2]; controls=0 [0;0]; $p = <0.001$) and tended to have a higher WMH volume (patients=0.54 ml [0.28;1.7]; controls = 0.27 ml [0.11;0.73]; $p = 0.11$). The number of microbleeds ($p = 0.41$) and SVD burden score $p = 0.25$) did not differ significantly between patients and controls (Table 2).

Within patients, no significant relations between perforating artery flow measures and SVD manifestations were found, although a lower CSO flow velocity ($r=−0.56$; $p = 0.06$) and BG flow velocity ($r=−0.43$; p

= 0.11) tended to be related to larger WMH volume (Table 6; and for controls sup. Table 2).

4. Discussion

In this exploratory study we found that several measures of cerebral perforating artery flow were unaffected in patients with carotid occlusive disease, although there were indications of reduced perforating artery flow velocity at the level of the CSO. Lower CSO artery flow velocity also tended to be associated with larger WMH volume in these patients and the same was found for artery flow velocity at the BG level.

Observed values for CSO perforating artery flow velocity and pulsatility of our controls correspond with previous findings in elderly healthy participants [12,21]. This is also true for the pulsatility values of perforating arteries in the BG [12,21]. BG flow velocities are slightly lower, likely due to the exclusion of non-perpendicular perforating arteries at this level in the current study. These are often larger vessels with higher velocities. A relatively large number of subjects was excluded due to poor scan quality resulting from subject movement during scanning (patients: 33% in CSO and 21% in BG; controls: 25% in CSO and 18% in BG). A previous study about perforating artery flow reported lower exclusion numbers due to subject motion (patients: 18% in CSO and 0% in BG; controls: 0% in CSO and 8% in BG) [15]. The difference may result from the slightly higher mean age of our cohort (64 vs. 59 years for patients; 65 vs. 61 years for controls), and this has been noted before in studies of perforating artery flow in older subjects [12]. This is a known phenomenon for older people which tend to move more during MRI scanning than younger people [22]. The burden of SVD manifestations in our patients with carotid occlusive disease was somewhat lower than previously described [11,23,24]. This may be caused by the lower age of our included patients and the fact that they are still independent in daily life, suggesting a patient cohort with relatively normal and stable hemodynamic function.

Carotid occlusive disease is characterized by hemodynamic impairments, such as decreased CBF and cerebrovascular reactivity, and lower perfusion pressure in the absence of sufficient collaterals [1–7]. These hemodynamic impairments can vary between carotid occlusive disease patients, depending on the degree of collateral flow and on the patient's hemodynamic stability, and is also reflected in ischemic symptoms. PET, MRI and transcranial Doppler measurements have shown that hemodynamic impairments are typically most pronounced in border zone areas, including the CSO and BG [3–6]. In patients with carotid occlusive disease, these regions also frequently present with low-flow infarcts (i.e. rosary-like infarctions) and WMH [8,9]. Previous research has shown that hemodynamic alterations as well as cerebral lesions are more common in the CSO than in other border zone regions [3–6,25]. These previous findings agree with lower flow velocity in the CSO perforating arteries in patients with carotid occlusive disease and its relation with WMH volume as observed in the present study. Hemispherical differences concerning hemodynamic impairments and lesion occurrence and severity in patients with carotid occlusive disease are not unambiguously shown in literature [9]. This agrees with the current finding that

Table 6
Relations between cerebral perforating artery flow and visible manifestation of small vessel disease in patients with carotid occlusive disease.

	Pulsatility CSO	Flow velocity CSO	Pulsatility BG	Flow velocity BG
SVD burden score	r = −0.06; p = 0.83	r = −0.37; p = 0.17	r = 0.09; p = 0.77	r = 0.08; p = 0.80
WMH volume (ml)	r = −0.30; p = 0.23	r = −0.56; p = 0.06	r = 0.05; p = 0.85	r = −0.43; p = 0.11

r = Spearman correlation coefficient. Abbreviations: CSO = semioval center; BG = basal ganglia; SVD = small vessel disease; WMH = white matter hyperintensity.

apart from lower M1 pulsatility, no differences between hemispheres were found in hemodynamic parameters of flow. Because we did not obtain an MR angiography of the circle of Willis, we cannot evaluate how patterns of collateral flow in the proximal arteries affect perforating artery flow measures.

Our results suggest that hemodynamic changes occur in the distal small perforating arteries of CSO border zone areas, which likely reflect the vulnerability of these regions in patients with carotid occlusive disease, despite the fact that our patients otherwise appeared to be relatively hemodynamically stable, being asymptomatic for the past period and also having normal flow in proximal arteries. Nevertheless, the hemodynamic changes in the small perforating arteries may be clinically relevant also in this setting as reflected in the relation with WMH volume. In light of these observations the question arises whether lower perforating artery flow and subcortical ischemic lesions in patients with carotid occlusive disease are a direct consequence of hemodynamic changes at the level of the carotid artery, or rather reflect co-occurring SVD. The latter can be due to shared risk factors between atherosclerosis and SVD [9,26]. Our research cannot distinguish between these two possibilities, but does indicate that hemodynamic changes in small perforating arteries may contribute to overall brain damage in patients with carotid occlusive disease.

Some limitations of our study need to be considered. First, the perforating arteries assessed in this study have sub-voxel sizes, indicating the presence of partial volume effects which generally lead to underestimation of the velocity and an overestimation of the pulsatility [12]. However, it appears unlikely that partial volume effect drive our results, because a drop in perfusion pressure and CBF has been shown to result in vasodilation in an attempt to maintain CBF [27]. Therefore, in patients with carotid occlusive disease, partial volume effects are expected to be less, leading to less velocity underestimation. Nevertheless, despite less velocity underestimation, results indicate lower flow velocities in patients with carotid occlusive disease. Furthermore, the statistical power of this study was limited. Therefore, we could only detect relations with medium or large effect. Limited power was due to i) the challenging acquisition of good quality 7T MRI data of the cerebral perforating arteries due a motion sensitive 2D CP sequence, reflected in the relatively small sample size included in the analysis; ii) even after optimization of the signal to noise ratio to the extent of what is currently feasible, the perforating artery flow measurements have a relatively large amount of noise, introducing measurement uncertainty; and iii) the inclusion of a reasonably hemodynamically stable subject cohort, reflected by the absence of symptoms three months prior to inclusion. In hemodynamically less stable subjects larger effects are expected to be found.

5. Conclusion

Our observations in a group of patients with carotid occlusive disease without recent ischemic symptoms, indicate that although several measures of cerebral perforating artery flow were unaffected, there were indications of reduced perforating artery flow velocity, particularly in the watershed areas, and reduced perforating artery flow velocity tended to be related to a higher burden of subcortical ischemic injury. This suggests that the small perforating arteries contribute to damage and possibly also to clinical outcome in patients with carotid occlusive disease. This offers value to future research into the small cerebral perforating arteries in larger cohorts and preferably longitudinal studies.

Disclosures

The authors have no conflicts of interest to declare.

Supplementary materials

Supplementary material associated with this article can be found, in the online version, at doi:10.1016/j.cccb.2022.100143.

References

[1] J. Hendrikse, M.J. Hartkamp, B. Hillen, et al., Collateral ability of the circle of willis in patients with unilateral internal carotid artery occlusion border zone infarcts and clinical symptoms, Stroke 32 (2001) 2768–2773, https://doi.org/10.1161/hs1201.099892.

[2] W.J. Powers, G.A. Press, R.L. Grubb, et al., The effect of hemodynamically significant carotid artery disease on the hemodynamic status of the cerebral circulation, Ann. Intern. Med. 106 (1987) 27–35, https://doi.org/10.7326/0003-4819-106-1-27.

[3] R. Leblanc, Y.L. Yamamoto, J.L. Tyler, et al., Hemodynamic and metabolic effects of extracranial carotid disease, J. Neurol. Sci. 16 (1989) 51–57, https://doi.org/10.1017/S031716710002850X.

[4] R.P.H. Bokkers, P.J. Van Laar, K.C.C. Van De Ven, et al., Arterial spin-labeling MR imaging measurements of timing parameters in patients with a carotid artery occlusion, Am. J. Neuroradiol. 29 (2008) 1698–1703, https://doi.org/10.3174/ajnr.A1232.

[5] H. Yamauchi, H. Fukuyama, Y. Nagahama, et al., Cerebral hematocrit decreases with hemodynamic compromise in carotid artery occlusion: a PET study, Stroke 29 (1998) 98–103, https://doi.org/10.1161/01.STR.29.1.98.

[6] M. Kluytmans, J. Van Der Grond, M.A. Viergever, Gray matter and white matter perfusion imaging in patients with severe carotid artery lesions, Radiology 209 (1998) 675–682, https://doi.org/10.1148/radiology.209.3.9844658.

[7] R.F. Leoni, K.C. Mazzetto-Betti, A.C. Silva, et al., Assessing cerebrovascular reactivity in carotid steno-occlusive disease using MRI BOLD and ASL techniques, Radiol. Res. Pract. 2012 (2012) 1–10, https://doi.org/10.1155/2012/268483.

[8] H. Krapf, B. Widder, M. Skalej, Small rosarylike infarctions in the centrum ovale suggest hemodynamic failure, Am. J. Neuroradiol. 19 (1998) 1479–1484.

[9] C.J.M. Klijn, L.J. Kappelle, C.A.F. Tulleken, et al., Symptomatic carotid artery occlusion: a reappraisal of hemodynamic factors, Stroke 28 (1997) 2084–2093, https://doi.org/10.1161/01.STR.28.10.2084.

[10] H. Baradaran, E.E. Mtui, J.E. Richardson, et al., Hemispheric differences in leukoaraiosis in patients with carotid artery stenosis: a systematic review, Clin. Neuroradiol. 27 (2017) 7–13, https://doi.org/10.1007/s00062-015-0402-2.

[11] C. Enzinger, S. Ropele, T. Gattringer, et al., High-grade internal carotid artery stenosis and chronic brain damage: a volumetric magnetic resonance imaging study, Cerebrovasc. Dis. 30 (2010) 540–546, https://doi.org/10.1159/000319025.

[12] L. Geurts, G.J. Biessels, P. Luijten, et al., Better and faster velocity pulsatility assessment in cerebral white matter perforating arteries with 7T quantitative flow MRI through improved slice profile, acquisition scheme, and postprocessing, Magn. Reson. Med. 79 (2018) 1473–1482, https://doi.org/10.1002/mrm.26821.

[13] M.A. Van Buchem, G.J. Biessels, H.P. Brunner La Rocca, et al., The heart-brain connection: a multidisciplinary approach targeting a missing link in the pathophysiology of vascular cognitive impairment, J. Alzheimer's Dis. 42 (2014), https://doi.org/10.3233/JAD-141542. Published online.

[14] A.M. Hooghiemstra, A.S. Bertens, A.E. Leeuwis, et al., The missing link in the pathophysiology of vascular cognitive impairment: design of the heart-brain study, Cerebrovasc. Dis. Extra 7 (2017) 140–152, https://doi.org/10.1159/000480738.

[15] L.J. Geurts, J.J.M. Zwanenburg, C.J.M. Klijn, et al., Higher pulsatility in cerebral perforating arteries in patients with small vessel disease related stroke, a 7T MRI study, Stroke 50 (2019) 62–68, https://doi.org/10.1161/strokeaha.118.022516.

[16] T. Arts, L.P. Onkenhout, R.P. Amier, et al., Non-invasive assessment of damping of blood flow velocity pulsatility in cerebral arteries with MRI, J. Magn. Reson. Imaging (2021), https://doi.org/10.1002/jmri.27989. Published online.

[17] T. Arts, J.C.W. Siero, G.J. Biessels, et al., Automated assessment of cerebral arterial perforator function on 7T MRI, J. Magn. Reson. Imaging (2021) 234–241, https://doi.org/10.1002/jmri.27304.

[18] R. de Boer, H.A. Vrooman, F. van der Lijn, et al., White matter lesion extension to automatic brain tissue segmentation on MRI, Neuroimage 45 (2009) 1151–1161, https://doi.org/10.1016/j.neuroimage.2009.01.011.

[19] J.M. Wardlaw, E.E. Smith, G.J. Biessels, et al., Neuroimaging standards for research into small vessel disease and its contribution to ageing and neurodegeneration, Lancet Neurol. 12 (2013) 822–838, https://doi.org/10.1016/S1474-4422(13)70124-8.

[20] J. Staals, T. Booth, Z. Morris, et al., Total MRI load of cerebral small vessel disease and cognitive ability in older people, Neurobiol. Aging 36 (2015) 2806–2811, https://doi.org/10.1016/j.neurobiolaging.2015.06.024.

[21] W.H. Bouvy, L.J. Geurts, H.J. Kuijf, et al., Assessment of blood flow velocity and pulsatility in cerebral perforating arteries with 7-T quantitative flow MRI, NMR Biomed. 29 (2016) 1295–1304, https://doi.org/10.1002/nbm.3306.

[22] H.R. Pardoe, R. Kucharsky Hiess, R Kuzniecky, Motion and morphometry in clinical and nonclinical populations, Neuroimage 135 (2016) 177–185, https://doi.org/10.1016/j.neuroimage.2016.05.005.

[23] E. Ammirati, F. Moroni, M. Magnoni, et al., Relation between characteristics of carotid atherosclerotic plaques and brain white matter hyperintensities in asymptomatic patients, Sci. Rep. 7 (2017) 1–11, https://doi.org/10.1038/s41598-017-11216-x.

[24] M.P. Lin, T.G. Brott, D.S. Liebeskind, et al., Collateral recruitment is impaired by cerebral small vessel disease, Stroke 51 (2020) 1404–1410, https://doi.org/10.1161/STROKEAHA.119.027661.

[25] S. Nakano, K. Yokogami, H. Ohta, et al., CT-defined large subcortical infarcts: correlation of location with site of cerebrovascular occlusive disease, Am. J. Neuroradiol. 16 (1995) 1581–1585.

[26] J.M. Wardlaw, C. Smith, M. Dichgans, Mechanisms underlying sporadic cerebral small vessel disease : insights from neuroimaging, Lancet Neurol. 12 (2013) 70060–70067, https://doi.org/10.1016/S1474-4422(13)70060-7.

[27] A.L. Gordon, S. Goode, O.D.' Souza, et al., Cerebral misery perfusion diagnosed using hypercapnic blood-oxygenation-level-dependent contrast functional magnetic resonance imaging: a case report, J. Med. Case Rep. 4 (2010), https://doi.org/10.1186/1752-1947-4-54.